# Structural Biological Materials: Overview of Current Research

P.-Y. Chen, A.Y.-M. Lin, A.G. Stokes, Y. Seki, S.G. Bodde, J. McKittrick, and M.A. Meyers

*Through specific biological examples this article illustrates the complex designs that have evolved in nature to address strength, toughness, and weight optimization. Current research is reviewed, and the structure of some shells, bones, antlers, crab exoskeletons, and avian feathers and beaks is described using the principles of materials science and engineering by correlating the structure with mechanical properties. In addition, the mechanisms of deformation and failure are discussed.*

## INTRODUCTION

The composition and structure of inorganic and organic components within nature's biological composites is often intimately connected to the different structural scale levels, creating a hierarchy that optimizes strength and toughness while minimizing weight for specific applications. The damage mechanisms in biological materials are far more sophisticated than current technological designs. One of the important differences is that nature does not have at its disposal the cornucopia of strong synthetic materials developed in the past century that rely, for the most part, on high-temperature processing. Thus, ingenious design has to be coupled with the ability to change shape and configuration during the life of the organism. Multifunctionality and self-healing ability are inherent characteristics of many of these components, which ensure survival in an environment where natural selection constantly 'tunes' them.

The Arzt pentahedron[1] shows schematically how the various elements that are unique to biological materials contribute to the structures. While the study of these biological materials per se is a fascinating field with plenty of challenges for materials scientists, materials engineers look at them with a keen eye for the multifunctionality and hierarchical structure of these materials that is a matter of life or death.Thus, evolution has played and continues to play a pivotal role in selecting the structures that offer optimum performance. Indeed, natural selection and evolutionary constraints constitute one of the vertices of the Arzt pentahedron. This article focuses on a few structural biological materials that are under study by the authors. The materials science approach that is illustrated here has proven to be very useful and is revealing features and properties heretofore not studied by other fields. This brief article represents the continuation of an earlier article published in *JOM*.[2] M. Meyers et al. provided greater detail and an in-depth overview.[3]

### How would you…

**…describe the overall significance of this paper?**

*This paper presents a description of the authors' latest studies of unusual structure/property relationships of various biological taxa.*

**…describe this work to a materials science and engineering professional with no experience in your technical specialty?**

*This paper is an overview of some of the structures and mechanical properties of natural biological materials.*

**…describe this work to a layperson?**

*This paper is an overview of the structure and strength of various biological materials such as seashells, crab exoskeletons, bird beaks, and deer antlers.*

## SHELLS

While there are a great variety of shells in the oceans and rivers, this study has focused on the conch,[4] abalone,[5–8] the Amazon River clam, and giant clam.[9] Notable studies on shells are the early works by J.F.W. Vincent,[10] V.J. Laraia et al.,[11] and M. Sarikaya et al.,[12,13] to name just a few. There are significant current efforts focused on elucidating the fundamental mechanisms of deformation and failure from the nanometer to the structural level.

Of the shells studied, abalone will be the focus here. The abalone shell has two layers: an outer prismatic layer (rhombohedral calcite) and an inner nacreous layer (orthorhombic aragonite). This inner layer has been intensely studied because of its excellent mechanical strength. Aragonitic $CaCO_3$ constitutes the inorganic component of the nacreous ceramic/organic composite (95 wt.% ceramic, 5 wt.% organic material). This composite is comprised of stacked platelets (~0.5 μm thick) arranged in a brick-and-mortar microstructure with an organic matrix (20–50 nm thick) interlayer that is traditionally considered as serving as glue between the single platelets. There is a high degree of crystallographic texture characterized by a nearly perfect "c-axis" alignment normal to the plane of the tiles.

Figure 1 shows (a) an abalone shell, (b) its mesostructure, and (c) its microstructure. The mesostructure (Figure 2a) is characterized by the presence of organic mesolayers which are due to growth cycle interruptions. These organic layers are themselves permeated with mineral, as shown in Figure 2b. The principal feature of the microstructure is the stacking of tiles with dimen-

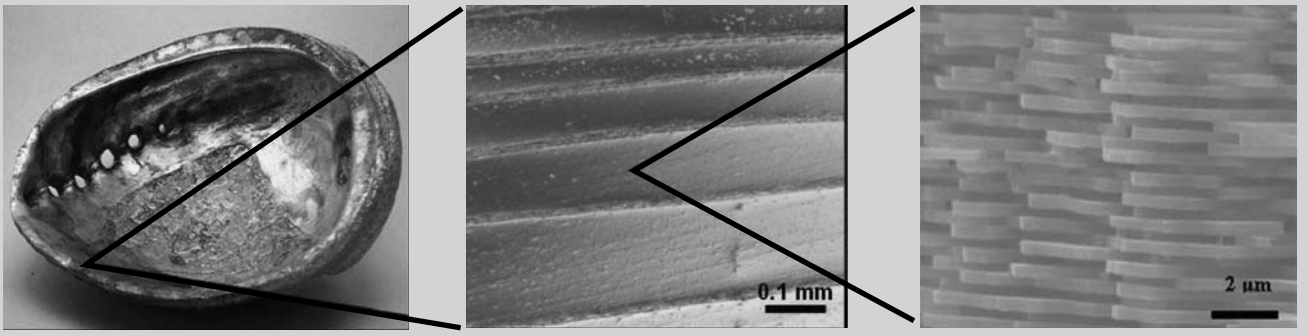


Figure 1. The hierarchical structure of abalone nacre. (a) An abalone shell, (b) its mesostructure, and (c) the aragonite tiles of its microstructure.

sions of 0.5 µm thickness and ~10 µm diameter. It will be seen below that they are connected by mineral bridges that play a pivotal role in mechanical strength and ensure growth in a quasi-monocrystal mode; subsequent layers have the same crystallographic orientation, as seen in Figure 3. Figure 3 illustrates that the crystallographic orientation of adjacent tile layers is the same. Similar transmission-electron microscopy (TEM) results had been obtained earlier by Sarikaya.[13]

The determination of the shell strength when the loading is applied perpendicular to its surface can directly address the role played by the organic layer. A dramatic difference in strength is found between the tensile and compressive strengths, much greater than in conventional brittle materials. The ratio between compressive and tensile strength is on the order of 50, whereas in brittle materials it varies between 8 and 12. This difference is indeed striking, especially if one considers the tensile strength parallel to the layer plane; it is on the order of 150–200 MPa, one third of the compressive strength. It can be concluded that the shell sacrifices tensile strength in the perpendicular direction to the tiles to use it in the parallel direction. Interestingly, the average of the tensile strength (in the perpendicular and parallel directions) is approximately 75–100 MPa, whereas the compressive strength is approximately 500 MPa. This is much closer to the 'normal' value for the ratio between compressive and tensile strength of ceramics. Figure 4 shows in a schematic fashion the compressive and tensile strengths collected from a variety of past studies,[5,12–16] both perpendicular and parallel to the shell surface. The ratio between the compressive and tensile strengths parallel to the surface, 3:5, is much smaller than that characteristic of ceramics.

Figure 5 shows, in schematic fashion, the failure mechanisms of abalone shells in different loading conditions: (a) tension parallel to shell surface, (b) shear parallel to shell surface, (c) compression parallel to shell surface, and (d) tension perpendicular to shell surface. When tension is applied parallel to the surface, the tiles slide past each other rather than fracturing. The mech-

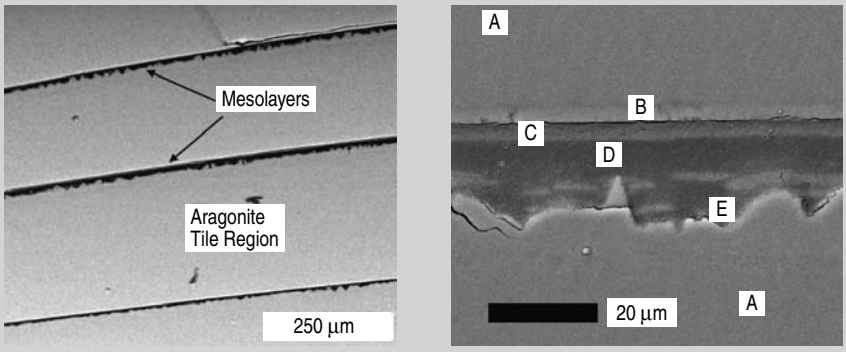


Figure 2. (a) A macrostructural view of a cross section of the Haliotis rufescens shell. Growth bands are observed separating larger regions of nacre. (b) An SEM micrograph of polished surface of mesolayers. Tiles (A): block-like calcite (B): organic/inorganic mix (C): organic (D): and spherulites (E) are observed.

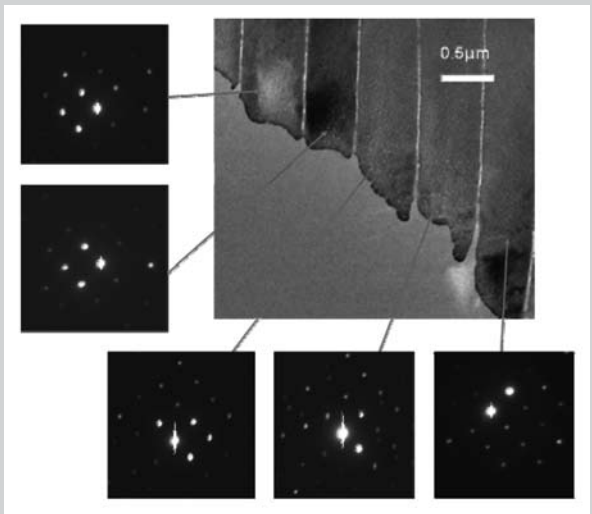


Figure 3. A TEM of abalone nacre tiles showing that crystallographic orientations of adjacent tiles in the same growth stack are identical.

anism of failure involves fracture of the mineral bridges and stretching of the organic.

Upon compression parallel to the plane of the tiles, an interesting phenomenon observed previously in synthetic composites was seen along the mesolayers: plastic microbuckling. This mode of damage involves the formation of a region of sliding and of a knee. Figure 6a shows a plastic microbuckling event in an Amazon River clam. Plastic microbuckling, which is a mechanism to decrease the overall strain energy, was observed in a significant fraction of the specimens. Plastic microbuckling is a common occurrence in the compressive failure of fiber-reinforced composites when loading is parallel to the reinforcement. The coordinated sliding of layer segments of the same approximate length by a shear strain $\gamma$ produces an overall rotation of the specimen in the region with a decrease in length. Figure 6b shows a characteristic microbuckling region found in abalone nacre. The angle $\alpha$ was measured and found to be approximately 35°. The ideal angle, which facilitates microbuckling according to Argon, is 45°.[17]

The low tensile strength is the direct result of the growth process, which involves the periodic deposition of organic layers that reduce the velocity of growth in the c direction of the orthorhombic aragonite structure and create the tile structure. It is possible to estimate the tensile strength of each individual mineral bridge and to calculate the overall tensile strength, from the density of these bridges. The mineral bridges have diameters in the nanometer range ( ~50 nm). Used here is an extension of the approach introduced by the Max Planck Institute (H.J. Gao et al.,[18] B.H. Ji and Gao,[19] and Ji et al.[20]) for biological materials. The classical fracture mechanics equation is applied to aragonite. The maximum stress, $\sigma_{fr}$, as a function of flaw size, 2a, can be estimated, to a first approximation, as shown in Equation 1, where $K_{Ic}$ is the fracture toughness. (All equations are given in the table.) However, the

**Equations**

$$\sigma_{fr} = \frac{K_{Ic}}{\sqrt{\pi a}} \quad (1)$$

$$\sigma_{th} = \frac{E}{30} \quad (2)$$

$$f = \frac{\sigma_t}{\sigma_{th}} \quad (3)$$

$$f = \frac{nA_B}{A_T} \quad (4)$$

$$n = \frac{\sigma_t A_T}{\sigma_{th} A_B} \quad (5)$$

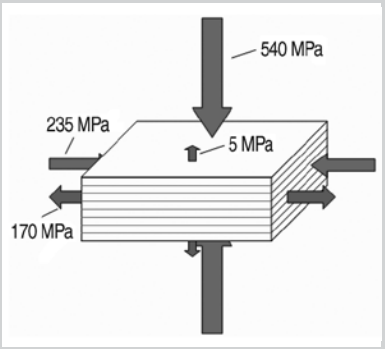


Figure 4. The compressive strength and ultimate tensile strength of nacre with respect to loading direction.

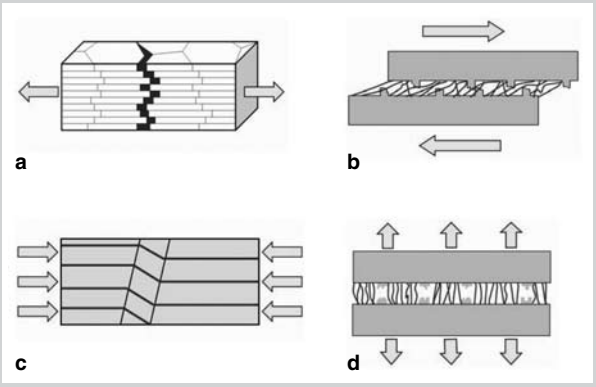


Figure 5. Failure mechanisms of abalone shells in different loading conditions: (a) tension parallel to shell surface, (b) shear parallel to shell surface, (c) compression parallel to shell surface, and (d) tension perpendicular to shell surface.

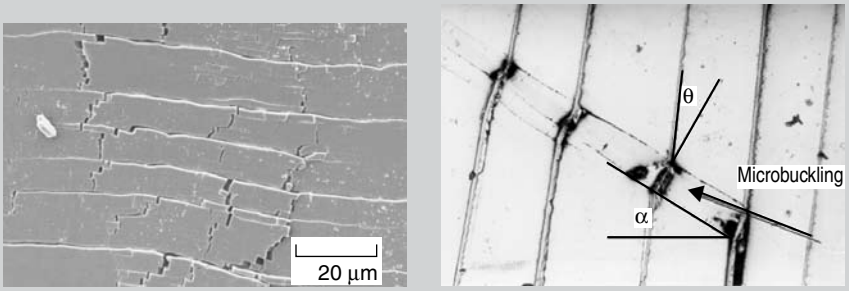


Figure 6. (a) A plastic microbuckling event in an Amazon River clam; (b) a characteristic microbuckling region found in abalone nacre.

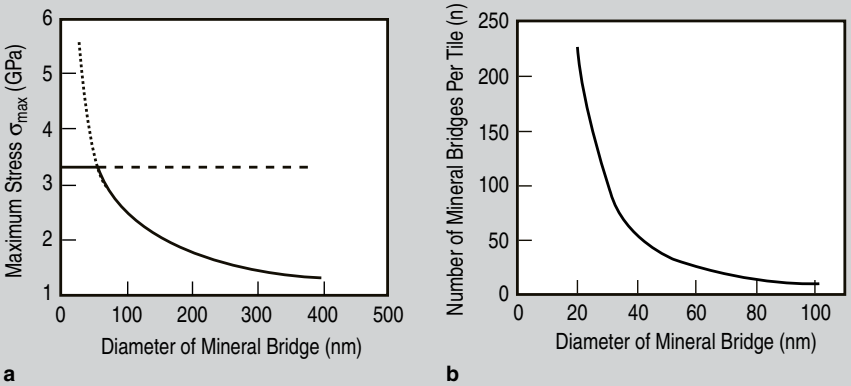


Figure 7. (a) The tensile strength of mineral as a function of size; (b) the calculated number of mineral bridges per tile as a function of bridge diameter.

strength is also limited by the theoretical tensile strength, which can be approximated as Equation 2 (Gao et al.[18]).

We assume that $K_{Ic}$= 1 MPa $m^{1/2}$, E = 100 GPa, and that 2a = D, where D is the specimen diameter. Figure 7a shows the two curves given by Equations 1 and 2. They intersect for a = 28 nm (D = 56 nm). This is indeed surprising, and shows that specimens of this and lower diameter can reach the theoretical strength. This is in agreement with the experimental results: the holes in the organic layer and asperities/bridge diameters are around 50 nm. It is possible to calculate the fraction of the tile surface consisting of mineral bridges, *f*. Knowing that the tensile strength is $\sigma_t$ and assuming that the bridges fail at $\sigma_{th}$, we have Equation 3.

The number of bridges per tile, n, can be calculated from Equation 4, where $A_B$ is the cross-sectional area of each bridge and $A_T$ is the area of a tile, resulting in Equation 5.

Assuming that the tiles have a diameter of 10 μm and that the bridges have a diameter of 50 nm (the approximate observed value), one obtains, for $\sigma_t$ = 3 MPa and $\sigma_{th}$ = 3.3 GPa, n = 36 as represented in Figure 7b. This result strongly suggests that mineral bridges can, by themselves, provide the bonding between adjacent tiles.

The number of asperities seen in surfaces of tiles greatly exceeds the values for bridges calculated herein. The estimated density is 60/μm$^2$. One conclusion that can be drawn is that a large number of asperities are indeed incomplete bridges and that these bridges are a small but important fraction of the protuberances.

## CRAB EXOSKELETONS

Arthropods are unique in that they have an exoskeleton, and not an endoskeleton like fishes, reptiles, and mammals. This exoskeleton is a multifunctional biological composite: it serves as attachment to the muscles, exchanges fluids with the environment, and offers protection against predators. In crustaceans (e.g., sheep crab studied by the authors[21] and the Maine lobster studied by the Max Planck Düsseldorf group[22–26])the primary constituents are chitin, proteins, and minerals.

In the horseshoe crab from which crustaceans evolved (this species has existed for 200 million years) there is an absence of mineralization and therefore the strength of the shell is considerably lower. Figure 8 shows the hierarchical structure of horseshoe crab (Limulus polyphemus) exoskeleton. The exoskeleton of horseshoe crabs is a sandwich composite consisting of three layers: an exterior shell, an intermediate layer, and an interior core. The exterior shell of a horseshoe crab is similar to crab exoskeletons with no mineral presence. Beneath the exterior shell is an intermediate layer consisting of vertical laminate about 2–3 μm wide that connects the exterior shell to the interior core. The interior core has an open-cell foam structure and is hollow in the middle. The cellular network is akin to the interior structure of toucan and hornbill beaks, as described in the following section. One of the fascinating aspects of horseshoe crabs is that the blood cells do not contain iron but copper; thus, they are true blue bloods. Their blood is harvested and used to

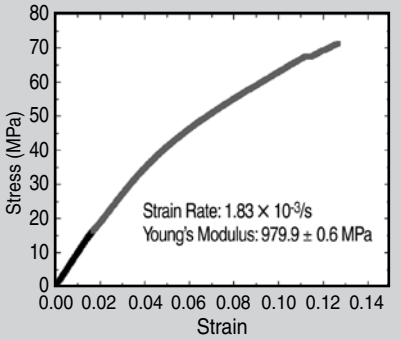


Figure 9. A typical stress-strain curve for American kestrel primary feather rachis is depicted. The data that appear in black are those used in determining Young's modulus.

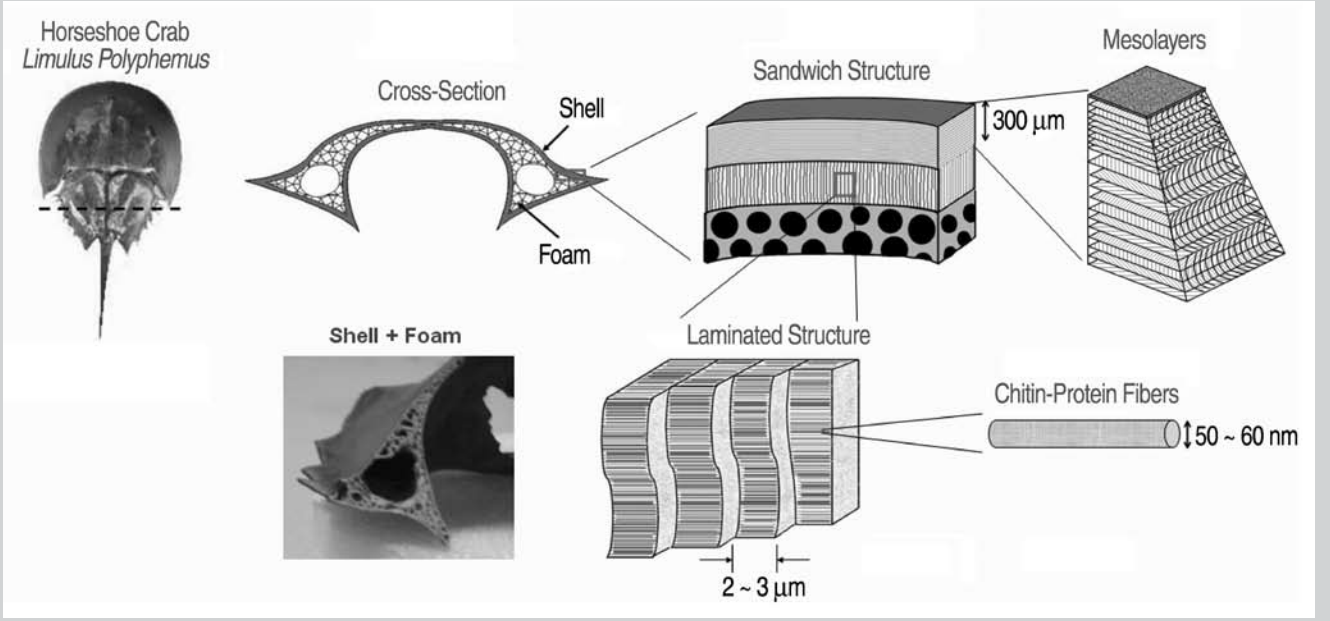


Figure 8. The hierarchical structure of the horseshoe crab exoskeleton.

test bacterial endotoxins in pharmaceutical and biomedical industries.

## AVIAN FEATHERS AND BEAKS

In the recent trend toward biomimetics, engineers have turned to what has attracted experimental biologists for decades already: avian appendages. Y. Seki et al.[27] described the bill of a Toco Toucan (Ramphastos toco) as a sandwich-structured composite, consisting of a closed-cell foam encased by this keratinous shell (ramphotheca). This model with inputs from data collected by tension and compression tests as well as hardness data was used to simulate the structure in flexure, for which foam-filled structures are optimized.

Previous and ongoing studies reveal analogous structure in the feather shaft (rachis). P. Purslow and J. Vincent[28] have quantified the morphology of primary feather rachis of pigeon (Columba livia) and in the context of mechanical properties. Consistent with the motif of cellular solid encased by cornified exterior, the feather rachis consists of a medulla foam enclosed in a relatively thin keratinous cortex. The medulla (Figure 10) can be described as a honeycomb structure. Based on preliminary analysis of micrographs, cell diameter is estimated to range from 10 μm to 30 μm.

Sections ranging in length from 1–2 cm have been excised from primary remiges of a single specimen of the American Kestrel (Falco sparevirus). Tensile testing is conducted at a fixed strain rate of 0.11/min. ($1.83 \times 10^{-3}$/s, corresponding to A. Taylor et al.[29] Based on preliminary results, the rachis of American Kestrel has a Young's modulus of approximately 1 GPa with ultimate tensile strength ranging from 40 MPa to 90 MPa. Figure 9 is representative of the mechanical response. Figure 10a and b depict scanning-electron micrographs (SEM) of the fracture surface corresponding to the data of Figure 9.

Beaks are composed of an ingenious sandwich structure and achieve ultralightweight construction. The face skin, ramphotheca, is made from β-keratin, which maintains a certain stiffness mainly for food gathering and functions as a protective barrier from natu-

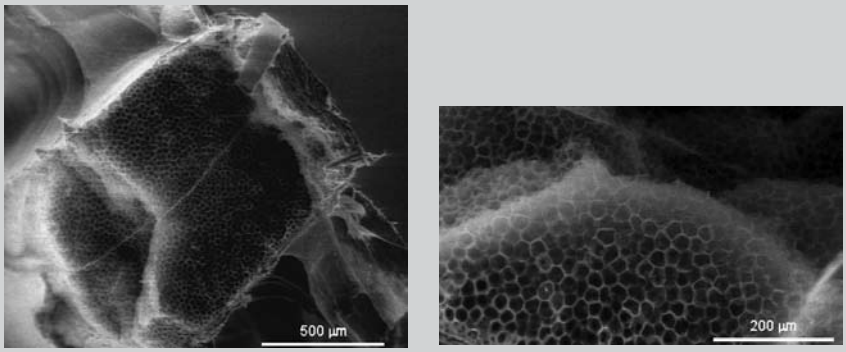


a b

Figure 10. Scanning-electron micrographs showing (a) the fracture surface of the American kestral primary feather rachis. Cleavage of the cellular solid is observed on ventral side of the rachis. (b) The mean diameter of honeycomb cells is approximately 20 μm.

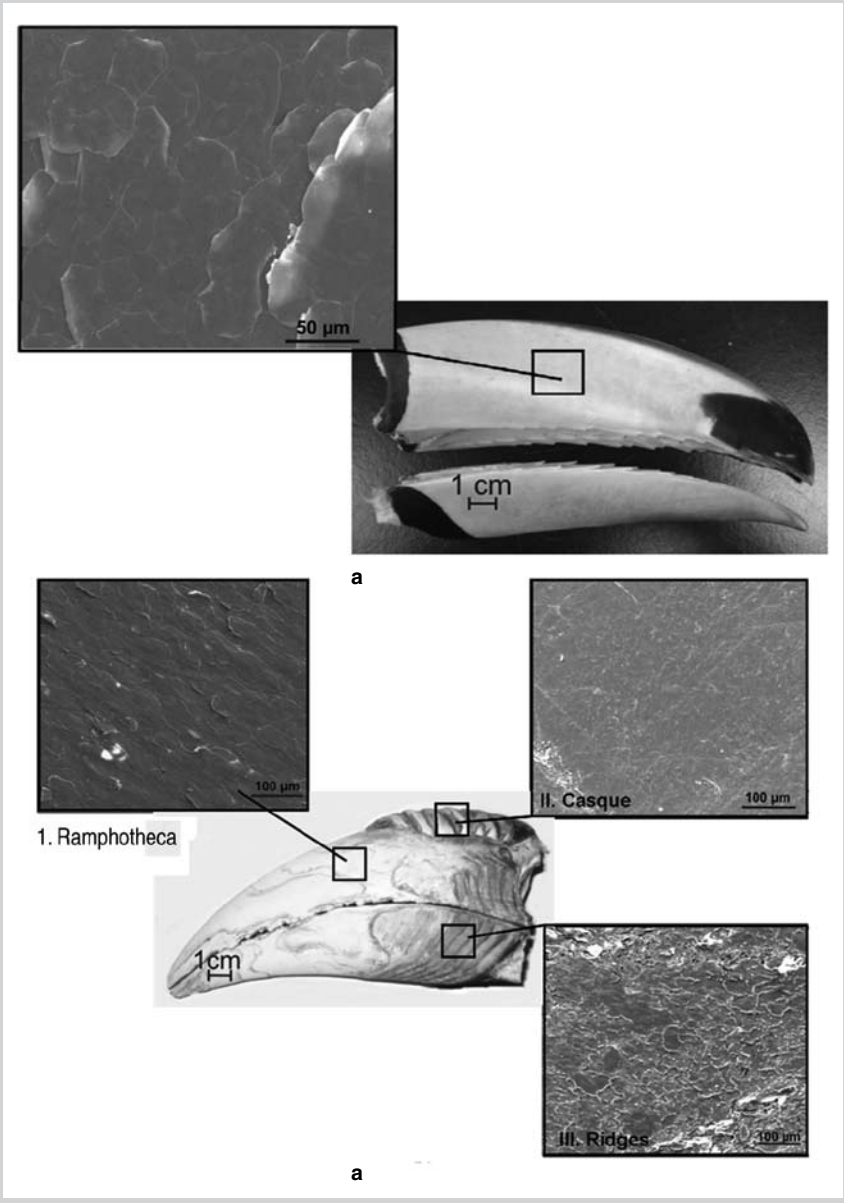


Figure 11. The structure of exterior beaks with scanning-electron micrographs of (a) toucan beak keratin and (b) hornbill beak keratin.

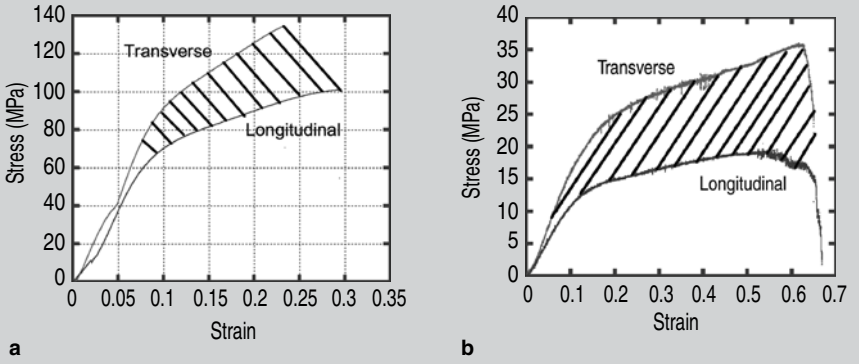


Figure 12. The stress-strain curves of toucan beak keratin; (a) 45% RH and 23ºC condition, (b) 95% RH and 38ºC condition.

ral environments. The internal foam core made from bone is an extension of a bird skull and is usually hollow at the center. The two entities are connected by the dermis. Most beaks are short and thick or long and thin. The toucan and hornbill beaks are unique; they are both long and thick. The toucan beak is 1/3 of the total length of the bird and the hornbill beak is 1/4 of the total length. The unique properties of the toucan and hornbill beaks motivated a recent study[27,30] and were investigated in relation to structure and mechanical properties. In previous studies, the mechanical properties of the Toco toucan beak have been investigated with analytical models in ambient condition. The finite element method is used to model the mechanical responses of the beak including the synergistic effect between the external shell and foam core. The authors have further evaluated the structure of beaks with computed tomography and the mechanical properties of toucan beak keratin at high humidity condition.

Figure 11 shows photographs and scanning-electron micrographs of Toco toucan and wreathed hornbill beak exteriors. Both beak keratins consist of multiple layers of keratin tiles. The toucan ramphotheca surface is constructed from a homogenous distribution of keratin tiles. The diameter of the tile is ~45 μm and the thickness of the tile is ~1 μm. The geometry of tiles is polygon and symmetric. Three types of ramphotheca surface are observed in the hornbill exterior keratin. The smooth surface is detected on hornbill ramphotheca and is similar to the toucan ramphotheca surface. The tile has a somewhat elongated shape and aligns in a certain direction.

The keratin tile structure on casque, a projection on maxillary, is not distinguishable and individual tile is tightly connected or merged with neighboring tiles. On the ridge surface, the connecting glue is observed in the keratin tile boundary region. The protruded glue differentiates surface morphology from the other two surfaces.

The mechanical properties of mammalian keratins are highly influenced by their moisture content.[31–33] In the case of avian keratins, the stiffness of feathers and claws at high humidity conditions significantly decreases.[34] The typical tensile stress-strain curves of toucan beak keratin under two conditions (23ºC and 45% relative humidity (RH), 38ºC and 95% RH) are shown in Figure 12. Under the low humidity condition, the Young's modulus of toucan keratin is isotropic in both directions, ranging from 1.04 ± 0.06 GPa (longitudinal) to 1.12 ± 0.13 GPa (transverse). The tensile strength of toucan beak keratin in the transverse direction was approximately 32% higher than in longitudinal direction shown in Figure 12a. The strength of toucan beak keratin significantly decreases under the high humidity condition shown in Figure 12b. The elongation at 95% RH exhibits approximately twofold higher than at 45% RH. The variation in strength in longitudinal and transverse directions is more distinctive under the high humidity. The average strength is 16.7 ± 2.2 MPa in longitudinal direction and 31.0 ± 4.4 MPa in transverse direction. The Young's modulus is 0.093 ± 0.02 GPa (longitudinal) and 0.17 ± 0.003 GPa (transverse). The stiffness in the high humidity condition drops by approximately an order of magnitude. The mass of hydrated keratin increases ~10% for 5 hours of exposure under 95% RH condition, which significantly decreases the mechanical properties of toucan beak keratin.

The toucan and hornbill foam cores consist of a closed-cell foam. The thin membranes cover individual cells composed of bony rods (trabeculae). The typical cell size of toucan foam is ~1 mm and that of hornbill foam is ~3 mm. The foam core increases the mechanical stability especially in the bending and energy absorption capacity of the beak, including the synergism between two components. The trabecu-

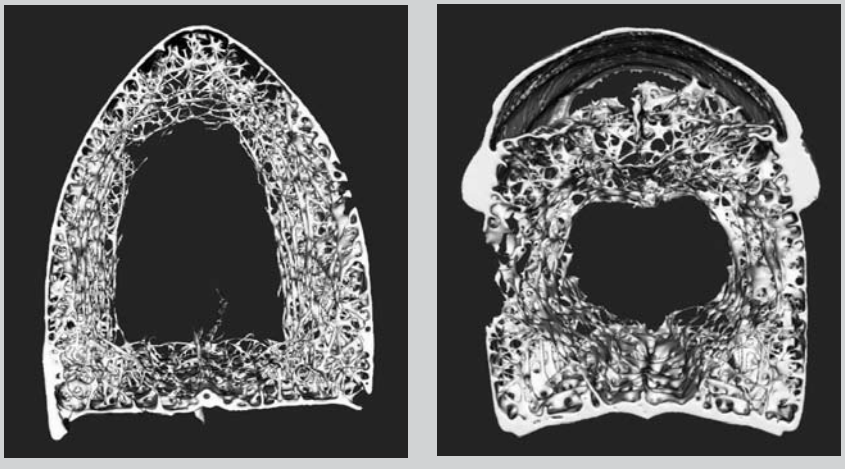


Figure 13. Three-dimensional models of beak foams; (a) toucan foam, (b) hornbill foam with keratin exterior.

a

b

Figure 14. Two elk bulls in Utah with antler locked after a fight. The downed animal died from exhaustion/dehydration. The photographer had to saw off the dead elk's antlers to free the live one. It is estimated that 10% of the bulls die during a battle. Photos courtesy of Prof. John Skedros, University of Utah.

lae of the toucan and hornbill are arranged in a complex manner and have high hardness in comparison with beak keratin. The microhardness or Vickers hardness of toucan and hornbill keratins is 0.22 ± 0.02 GPa and 0.21 ± 0.07 GPa (smooth surface), respectively, at atmospheric condition. The microhardness of toucan and hornbill foam materials is 0.28 ± 0.04 GPa and 0.39 ± 0.01 GPa. The microhardness of hornbill trabecula is comparable to avian bone.[35] The beak foams collapse in a brittle manner and fail by the buckling of rods in compression.

The complex foam interior structure is reconstructed by the three-dimensional (3-D) visualization techniques. The authors have used 200 image slices from micro-computed tomography at 93 μm resolution. Digital Data Viewer and Visualization Toolkit were used to generate isosurface mesh by using a marching cube algorithm.[36] The DICOM format of images is converted to .tiff format by ImageJ. In this study, the authors took half the size of the original image dataset (hornbill, 505 × 555, and toucan, 450 × 505) and doubled its size in the visualization process. Figure 13 shows the 3-D structure of toucan and hornbill foams. For the toucan, 1,372,890 mesh elements and for the hornbill, 1,799,760 were used to create the contour surface. The exterior of the toucan is eliminated and only bony foam is reconstructed. The hornbill foam includes exterior keratin and a secondary hollow is observed between bony foam and casque, shown in Figure 13b. The models clearly show the hollow structure of foam cores. The beak foams consist of a thin-walled structure with an interconnected network of the rods. The membranes disappeared from the models due to the low intensity of the membranes in computed tomography (CT) images.

## ANTLERS AND BONES

Antlers are one of the most impact-resistant and energy-absorbent of all biomineralized materials. They are one of the fastest-growing tissues in the animal kingdom, growing as much as 14 kg in 6 months, with a peak growth rate of up to 2–4 cm/day.[36] The antler is the only mammalian bone that is capable of regeneration, and thus offers unique insights into bone mineralization and growth. Antlers have two primary functions: they serve as visual signs of social rank within bachelor groups[37–40] and are used in combat, both as a shield and as a weapon.[37] The antlers have been designed to undergo high-impact loading and large bending moments without fracture. The unusual strength of antlers is attested by the very few observations of antler breakage during fighting in large groups of caribou and moose.[38] Figure 14 shows the aftermath of one battle, in which one bull died from exhaustion/dehydration (not wounds). The antlers between the live and dead bulls were tightly interlocked so that the live animal could not free itself, even by repeated pushing and tugging with ~400 kg of body

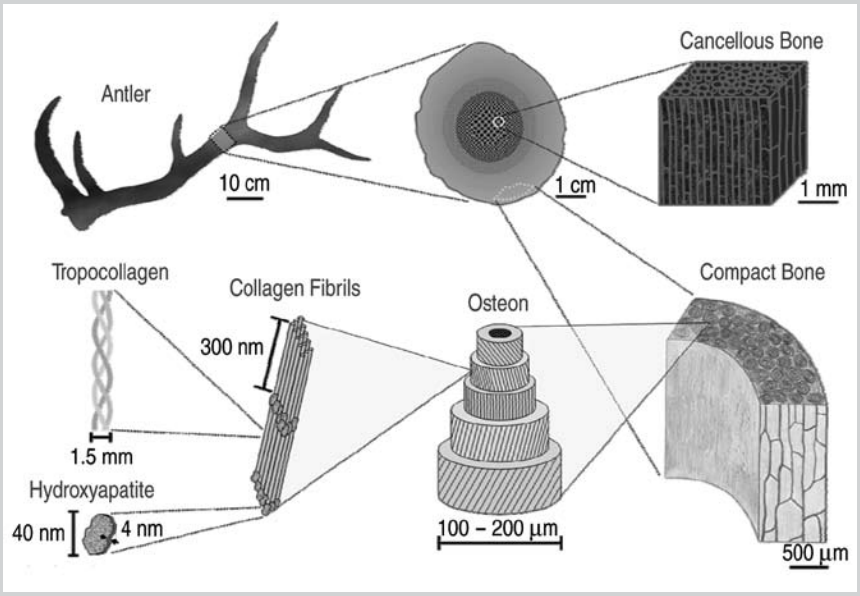


Figure 15. The hierarchical structure of antlers.

mass. The antlers from the dead animal had to be sawed off to free the live bull. Antlers are deciduous and are cast off (dropped) at the end of the rut, thus the age of the cast antler is ~7–9 months.

Antlers have a composition and microstructure very similar to other mammalian bones but there are distinct variations due to the functional differences between the tissues. Bones provide structural support and protection of organs whereas antlers provide neither. Given the long, slender appearance of most antlers, the natural comparison is to mammalian long bones. Long bones are hollow and contain interior fluids (blood, marrow, etc.). Bones produce vital cells and minerals necessary for the body whereas antlers remove fluids and minerals from the body in order to grow. Antlerogenesis (antler growth) requires a large amount of calcium and phosphorus in a short period of time. Red deer (Cervus elaphus, a European deer almost identical to the North American elk, Cervus canadensis) antlers require ~100 g/day of bone material in order to grow in comparison to growing fawn skeletons that take ~34 g/day.[41] This quantity of minerals cannot be obtained through food sources and has been shown to come from the skeleton of the animal.[36,41,42] The long bones of the legs and the ribs are the richest source, and are found to decrease in density as the antlers increase in size.[42] Thus, structural bone resorption occurs alongside antler bone remodeling during antlerogenesis. Another difference is that antlers are less mineralized than bone, and are one of the least mineralized of all biomineralized tissue.[43]

**Table I. Summary of Mechanical Properties of North American Elk Antler Compared to Bovine Femur**

| Property | Elk Antler | Ref. | Bovine Femur | Ref. |
|---|---|---|---|---|
| Density (g/cm$^3$) | 1.72 | 55 | 2.06 | 47 |
| Mineral Content (% ash) | 54.8 | 55 | 67 | 47 |
| Porosity (%) | 9.1 | 55 | 5.8 | 48,49 |
| Elastic Modulus (GPa) | 7.6 | 56 | 13.5 | 47 |
| Bending Strength (MPa) | 197 | 56 | 247 | 47 |
| Compressive Strength (MPa) | 126 | 56 | 254 | 57 |
| Fracture Toughness (MPa·m$^{1/2}$) | 11.0 | 56 | 2.1–5.2 | 58–60 |

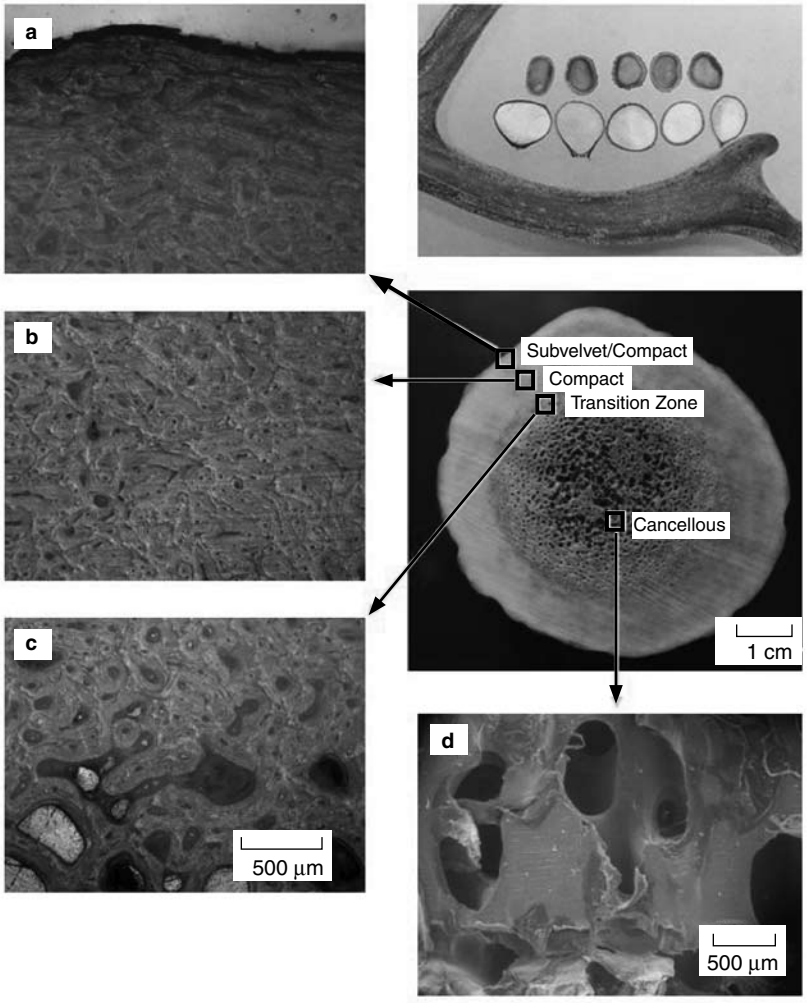


Figure 16. An antler cross section showing optical micrographs of the (a) subvelvet/compact interface, (b) compact, (c) transition (compact to cancellous) zone, and (d) a SEM micrograph of the cancellous bone.

Figure 15 shows the hierarchical structure of antlers. Antlers contain a core of trabecular (cancellous) bone surrounded by compact bone that runs longitudinally through the main beam of the antler and the prongs. The trabecular bone is somewhat anisotropic, with aligned channels directed parallel to the long axis of the antler beam. Compact bone surrounds this core, consisting of osteons that have a laminated structure of concentric rings extending from the main vascular channel. The concentric rings contain aligned collagen fibrils that have the mineral, hydroxyapatite (or more specifically dahllite), dispersed on or between the fibrils. The alignment of the collagen fibrils changes direction between the individual lamellae.

A cross section, perpendicular to the growth of an antler from an American elk, is shown in Figure 16, identifying the four main regions radiating outward from the center: cancellous, a transition zone between cancellous and compact bone, compact bone, and the subvelvet.[44] Optical micrographs show the subvelvet to be 100–150 µm thick with the transition region to compact bone notable for the low density of osteons.

Moving from the compact bone to the cancellous bone shows an increase in the size of the porosity, with the pore size ranging from 300 μm at the compact/cancellous interface to several millimeters at the interior of the cancellous region. The volume fraction of the cancellous bone is ~0.4 of the total volume.

Figure 17 shows optical micrographs of cross sections taken from the compact bone of the antler and a bovine femur. The antler shows osteons (100–225 μm diameter), Volkmann canals, vascular channels (15–25 μm diameter), and lacunae spaces (~10 μm diameter), as indicated on the micrograph. The majority of the osteons appear to be aligned along the growth direction. Depending on the age of the bone, human osteons range from 200–300 μm, substantially larger than what is found in the antler. This is likely due to the age difference between the reported values for human bone, typically taken on adults, as opposed to what is found in the relatively young antler.

Two types of osteons can be present in bone: primary and secondary. Primary osteons contain vascular channels surrounded by concentric bone lamellae. Primary osteons are generally smaller, do not have a cement line surrounding them and are embedded in layers of interstitial or circumferential bone. The cement line has been shown recently to be mineral rich, in contrast to earlier conclusions that the region was mineral poor.[45] Secondary osteons result from bone remodeling and often intersect each other and have a more rounded, uniform shape than primary osteons. J.D. Currey and others have pointed out that primary osteons are stronger than secondary osteons.[46,47] We could not completely distinguish between the two types in the micrograph, however the majority appear to be primary osteons, since they show a somewhat distorted cross section. Secondary osteons often arise in response to mechanical stress. Because an antler does not undergo mechanical forces during the growth process and only spends 1–2 months in sporadic (if at all) combat, it seems unlikely that secondary osteons would be present in a large amount in antlers. The antler porosity is estimated to be ~9.1% by volume, counting the vascular channels and lacunae void spaces.

The osteons in the bovine femur are more sparsely distributed compared to those in the antlers. These appear to be secondary osteons, given the uniform, circular shape of the majority. These osteons are embedded in parallel fiber (interstitial) bone, which is continually remodeled to form secondary osteons. Several elongated pores are observed, which actually are sections of the Volkmann canals, also appearing in the antler micrograph, along with the lacunae. The void space is estimated to be 5.1%, in agreement with a porosity of 5.8% measured in other bovine femora.[48,49] The interstitial bone has a higher

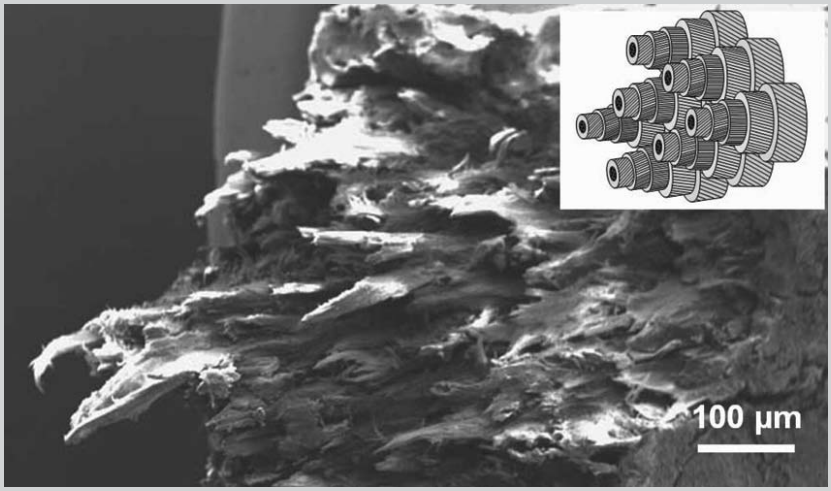


Figure 18. A scanning-electron micrograph of the fracture surface of a longitudinal specimen broken in bending, showing the fibrous nature of the fracture.

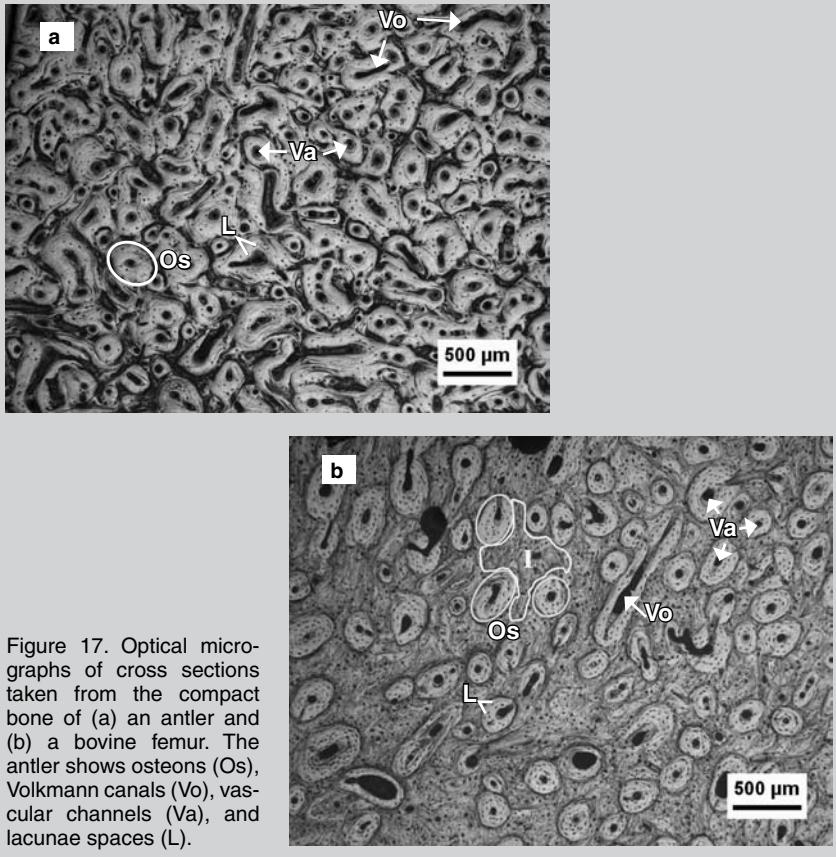


Figure 17. Optical micrographs of cross sections taken from the compact bone of (a) an antler and (b) a bovine femur. The antler shows osteons (Os), Volkmann canals (Vo), vascular channels (Va), and lacunae spaces (L).

strength and elastic modulus than secondary osteonal bone,[50] with an average modulus of ~27 GPa for mixed bone, similar to what was reported by others.[51,52] In the femur, ~41% by area are the secondary osteons.

While the mechanical properties of human and bovine bone have been highly documented, little data exists on the mechanical properties of antlers. North American elk antler was put through a variety of tests (bending, compression, and fracture toughness) to determine various mechanical properties. The results of these tests are compared to known data of bovine femur, summarized in Table I. The antler showed smaller values of density, amount of mineralization, elastic modulus, and strength; however, the antler had a higher fracture toughness. The elastic modulus and strength of bone scales with the mineral content,[53] which is consistent with the results presented here. The interstitial bone has a higher elastic modulus than the secondary osteons.[52,54] Thus, although primary osteons have a higher modulus than secondary ones, they are still not as stiff as interstitial bone, which is why the antler has a lower modulus. The higher fracture toughness of antlers correlates to their main function of having high impact resistance. The decrease in strength, however, is relatively small when considering the much faster growth rate of antlers. The fracture surface of an antler specimen fractured in three-point bending is shown in Figure 18. The fibrous nature of the fracture surface is observed, showing pullout of the osteons. The bending samples did not fracture completely; they failed gracefully with a large strain to failure, similar to a fiber-reinforced composite.

## ACKNOWLEDGEMENTS

*We gratefully acknowledge support from Professor Falko Kuester, Jackie Corbeil for CT scan, and Evelyn York for scanning electron microscopy. The curator of birds at the San Diego Zoo's Wild Animal Park kindly provided us with hornbill beaks. Mr. Jerry Jennings, owner of Emerald Forest Bird Gardens, has helped us immensely with the toucan beaks. We thank Project Wildlife for cooperation in providing specimens of American Kestrel for this study. We also thank Prof. Paul Price (UCSD) and Prof. John Skedros (University of Utah) for helpful discussions on bone. This research was funded by the National Science Foundation, Division of Materials Research, Biomaterials Program (Grant DMR 0510138).*

## References

1. E. Arzt, Mater. Sci. Eng. C, 26 (2006), pp. 1245–1250.
2. M.A. Meyers et al., *JOM,* 58 (7) (2006), pp. 35–41.
3. M.A. Meyers et al., *PMS,* 53 (2008), pp. 1–206.
4. R. Menig et al., *Mater. Sci. Eng. A,* 297 (2001), pp. 203–211.
5. R. Menig et al., *Acta Mater.,* 48 (2000), pp. 2383–2398.
6. A. Lin and M.A. Meyers, *Mater. Sci. Eng. A,* 390 (2005), pp. 27–41.
7. M.A. Meyers et al., *J. Mech. Behav. Biomed. Mat.*, 1 (2008), pp. 76–85.
8. A.Y.M. Lin, P.Y. Chen, and M.A. Meyers, *Acta Biomat.,* 4 (2008), pp. 131–138.
9. A.Y.M. Lin, M.A. Meyers, and K.S. Vecchio, *Mater. Sci. Eng. C*, 26 (2006), pp. 1380–1389.
10. J.F.W. Vincent, *Structural Biomaterials* (Princeton, NJ: Princeton University Press, 1991).
11. V.J. Laraia and A.H. Heuer. *J. Amer. Ceram. Soc.,* 72 (1989), pp. 2177–2179.
12. M. Sarikaya et al., *Mater. Res. Soc.,* 174 (1990), pp. 109–116.
13. J.D. Currey, *Proc. Roy. Soc. London,* 196 (1977), pp. 443–463.
14. A.P. Jackson, J.F.V. Vincent, and R.M. Turner, *Proc. Roy. Soc. London B,* B234 (1988), p. 415.
15. A.P. Jackson, J.F.V. Vincent, and R.M. Turner, *Comp. Sci. & Tech.,* 36 (1989), pp. 255–266.
16. M. Sarikaya, *Micro. Res. Tech.* (27) (1994), pp. 360–375.
17. A.S. Argon, *Fracture of Composites. Treatise of Materials Science and Technology* (New York: Academic Press, 1972), p. 1.
18. H.J. Gao et al., *Proc. Natl. Acad. Sci. USA,* 1000 (2003), pp. 5597–5600.
19. B.H. Ji and H.J. Gao, *J. Mech. Phys. Solid,* 52 (2004), pp. 1963–1990.
20. B.H. Ji, H.J. Gao, and K.J. Hsia, *Phil. Mag. Lett.,* 84 (2004), pp. 631–641.
21. P.Y. Chen et al., *Acta Biomater.*, 4 (2008), pp. 587–596.
22. D. Raabe et al., Mater. Sci. Forum, 495-97 (2005), pp. 1665–1674.
23. D. Raabe et al., *J. Crystal Growth,* 283 (2005) pp. 1–7.
24. D. Raabe, C. Sachs, and P. Romano, *Acta Mater.,* 53 (2005), pp. 4281–4292.
25. D. Raabe et al., *Mater. Sci. Eng. A,* 421 (2006), pp. 143–153.
26. C. Sachs, H. Fabritius, and D. Raabe, *J. Mater. Res.,* 21 (2006), pp. 1987–1995.
27. Y. Seki, M.S. Schneider, and M.A. Meyers, *Acta Materialia,* 53 (December 2005), pp. 5281–5296.
28. P.P. Purslow and J.F.V. Vincent, *Journal of Experiment Biology,* 72 (1978), pp. 251–260.
29. A.M. Taylor, R.H.C. Bonser, and J.W. Farrent, *Journal of Materials Science,* 39 (2004), pp. 939–942.
30. Y. Seki et al., *Mat. Sci. and Eng. C,* 26 (2006), pp. 1412–1420.
31. A. Kitchener and J.F.V. Vincent, *J. Mat. Sci.,* 22 (1987), pp. 1385–1389.
32. K.S. Wu, W.W. van Osdol, and R.H. Dauskardt, *Biomaterials,* 27 (2006), pp. 785–795.
33. J.E.A. Bertram and J.M. Gosline, *J. Exp. Biol.,* 130 (1987), pp. 121–136.
34. A.M. Taylor, R.H.C. Bonser, and J.W. Farrent, *J. Mat. Sci.,* 39 (2004), pp. 939–942.
35. R.H.C. Bonser, *J. Exp. Biol.,* 198 (1995), pp. 209–212.
36. R.J. Goss, *Deer Antlers: Regeneration, Function and Evolution* (New York: Academic Press, 1983).
37. V. Geist, *Behavior*, 27 (1966), pp. 175–214.
38. J. Henshaw, *Nature*, 231 (1971), p. 469.
39. G.A. Lincoln, *J. Exp. Zool.*, 182 (1972), pp. 233–249.
40. T.H. Clutton-Brock, *Behavior*, 79 (1982), pp. 108–124.
41. D.I. Chapman, *Mamm. Rev.*, 5 (1975), pp. 121–172.
42. W. Meister, *Anat. Rec.*, 1241 (1956), pp. 709–772.
43. J.D. Currey, *J. Biomech.*, 12 (1979), pp. 313–319.
44. H.J. Rolf and A. Enderle, *Anat. Rec.*, 255 (1999), pp. 69–77.
45. J.G. Skedros et al., *Anat. Rec. A*, 286 (2006), pp. 781–803.
46. S. Saha and W.C. Hayes, *Calcif. Tiss. Res.*, 24 (1977), pp. 65–72.
47. J.D. Currey, *Bones, Structure and Mechanics* (Princeton, NJ: Princeton University Press, 2002).
48. R.B. Martin and D.L. Boardman, *J. Biomech.,* 26 (9) (1993), pp. 1047–1054.
49. J.H. Kim, M. Niinomi, and T. Akahori, *Mater. Sci. Forum*, 475-479 (2005), pp. 2407–2410.
50. D.T. Reilly, A.H. Burnstein, and V.H. Frankel, *J. Biomech.*, 7 (1974), pp. 271–275.
51. W. Bonfield and P.K. Datta, *J. Biomech.*, 7 (1974), pp. 147–149.
52. D.T. Reilly and A.H. Burstein, *J. Biomech.,* 8 (1974), pp. 393–405.
53. J.D. Currey, *J. Biomech.*, 21 (1988), pp. 131–139.
54. J.Y. Rho et al., *Bone*, 25 (1999), pp. 295–300.
55. P.-Y Chen et al., *J. Mech. Prop. Behav. Biomed. Mater.*, accepted (in press).
56. P.-Y. Chen, A.G. Stokes, and J. McKittrick, *Acta Biomater.* (2008), in progress.
57. D.T. Reilly and A.H. Burstein, *J. Bone Joint Surg. Am.*, 56 (1974), pp. 1001–1022.
58. T.M. Wright and W.C. Hayes, *J. Biomech.,* 10 (1977), pp. 419–430.
59. W. Bonfield, M.D. Grynpas, and R.J. Young, *J. Biomech.,* 11 (1978), pp. 473–479.
60. P. Lucksanambool et al., *Biomaterials,* 22 (2001), pp. 3127–3132.

**P.-Y. Chen , A.Y.-M. Lin, A.G. Stokes, Y. Seki, S.G. Bodde, J. McKittrick, and M. A. Meyers, are with the University of California, San Diego. P.-Y. Chen can be reached at pochen@ucsd.edu.**